# A Conical Intersection Controls the Deactivation of the Bacterial Luciferase Fluorophore**

Samer Gozem, Ekaterina Mirzakulova, Igor Schapiro, Federico Melaccio, Ksenija D. Glusac,* and Massimo Olivucci*

Abstract: *The photophysics of flavins is highly dependent on their environment. For example, 4a-hydroxy flavins display weak fluorescence in solution, but exhibit strong fluorescence when bound to a protein. To understand this behavior, we performed temperature-dependent fluorescent studies on an N(5)-alkylated 4a-hydroxy flavin: the putative bacterial luciferase fluorophore. We find an increase in fluorescence quantum yield upon reaching the glass transition temperature of the solvent. We then employ multiconfigurational quantum chemical methods to map the excited-state deactivation path of the system. The result reveals a shallow but barrierless excited state deactivation path that leads to a conical intersection displaying an orthogonal out-of-plane distortion of the terminal pyrimidine ring. The intersection structure readily explains the observed spectroscopic behavior in terms of an excited-state barrier imposed by the rigid glass cavity.*

Oxidized flavin cofactors like flavin mononucleotide (FMN) contain a planar, stiff flavin moiety that displays intense fluorescence in solutions (with a lifetime of ca. 5 ns).[1] Such a fluorescence is quenched when the cofactor is protein-bound due to fast excited-state electron transfer from the flavin to neighboring aromatic amino acid residues (such as tyrosine or tryptophan). This behavior of oxidized flavins has been exploited to follow the conformational changes of flavoproteins over the course of enzymatic reactions.[2–5] In contrast, the 1,5 and 4a,5 flavin adducts (see Scheme 1 a) such as those found in reduced (FMNH$_2$)[6] and 4a-hydroxylated
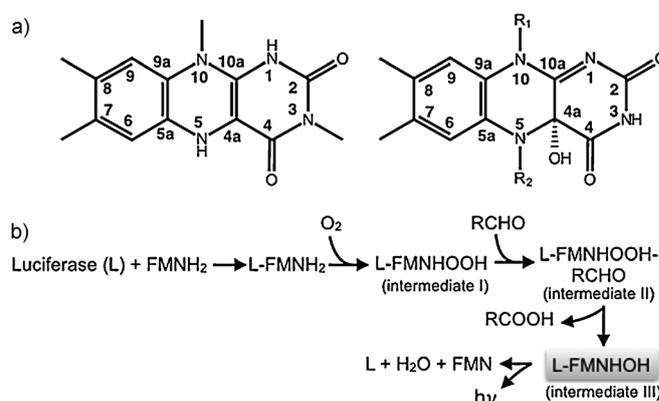
Scheme 1. a) Structures of the flavin chromophore in 1,5-reduced FMNH$_2$ (left) and the 4a-hydroxylated flavin adduct in FMNHOH (right). R$_2$ = H (in natural 4a-hydroxy flavin), R$_1$ = R$_2$ = CH$_2$CH$_3$ (in Et-FlOH), and R$_1$ = R$_2$ = CH$_3$ (in Me-FlOH, namely, 7,8-dimethyl-5,10-*N*-dimethyl-4a-hydroxyisoalloxazine). b) Proposed mechanism of bioluminescence in bacterial luciferase. Adapted from Ref. [15]. See also Figure S1 in the Supporting Information (SI).

(FMNHOH) cofactors, respectively,[7] display a weak fluorescence in solution.[8,9] However, when the same cofactors are protein-bound, the confinement[6,7] leads to an enhanced fluorescence emission.[10–15] The exact geometry and electronic structure of the emitting conformer and the mechanism preventing the efficient internal conversion occurring in solution are presently unknown.

A spectacular manifestation of the effects of protein confinement on flavin cofactors is seen in bacterial luciferases where a 4a,5 flavin adduct is held responsible for the bioluminescence of a vast group of marine eubacteria. In organisms such as *Vibrio harveyi*, the emission of the fluorophore may be strong enough to cause a blue luminescence of the microbial population that is so intense as to be observable from satellites.[16] Moreover, such flavin adducts are frequent intermediates in enzymatic catalysis by flavin-based monooxygenases, which activate molecular oxygen and catalyze the insertion of atomic oxygen into a number of substrates (e.g. in hydroxylations, sulfoxidations, epoxidations and Baeyer–Villiger oxidations).[17] A specific type of such monooxygenase activity is responsible for the bacterial luciferase fluorescence,[18–22] where the oxidation of aldehydes to acids via molecular oxygen would generate the 4a-hydroxy flavin byproduct as the putative light-emitting intermediate (FMNHOH in Scheme 1 b).[22,23]

Below we use complementary spectroscopic and computational methods to show that a 4a-hydroxy flavin is an

[*] Dr. S. Gozem,[+] Dr. E. Mirzakulova,[+] Dr. I. Schapiro,
Prof. Dr. K. D. Glusac, Prof. Dr. M. Olivucci
Chemistry Department, Bowling Green State University
Bowling Green, OH 43403 (USA)
E-mail: kglusac@bgsu.edu
    molivuc@bgsu.edu
Homepage: http://www.bgsu.lcpp.com/

Dr. F. Melaccio, Prof. Dr. M. Olivucci
Department of Biotechnology, Chemistry and Pharmacy
Università di Siena, via A. Moro 2, 53100 Siena (Italy)

[+] These authors contributed equally to this work.

Supporting information for this article is available on the WWW under http://dx.doi.org/10.1002/anie.201404011.

effective fluorophore when confined in an environment capable to prevent out-of-plane deformations of its terminal pyrimidine ring. More specifically, we demonstrate that when such a deformation is impaired the 4a-hydroxy flavin moiety is not able to access a conical intersection (CI) mediating the internal conversion of the emitting state.

Since the natural 4a-hydroxy flavin is unstable in the protein-free state, N(5)-alkylated 4a-hydroxy flavins (such as Et-FlOH in Scheme 1 a) are frequently used as experimental models for flavin-based bioluminescence. While these compounds are fluorescent in the protein[15] their fluorescence is weak when unbound. Using femtosecond pump–probe spectroscopy, we found that, in solution, the first singlet excited (S_1) state of Et-FlOH decays to the ground (S_0) state with several time constants but with a dominant component that has a 500 fs lifetime.[11]

The absorption spectrum of Et-FlOH in 2-methyl-tetra-hydrofuran (2-MeTHF) exhibits three bands in the UV region with λ_{max} at 282, 308 and 347 nm (Figure 1 a). All three absorption bands were assigned, on the basis of TDDFT calculations in acetonitrile, to π,π^* transitions with a degree of charge transfer character.[11] Similar bands were observed for other model 4a,5 flavin adducts whose energies were found to depend on the nature of substituents.[6,24]
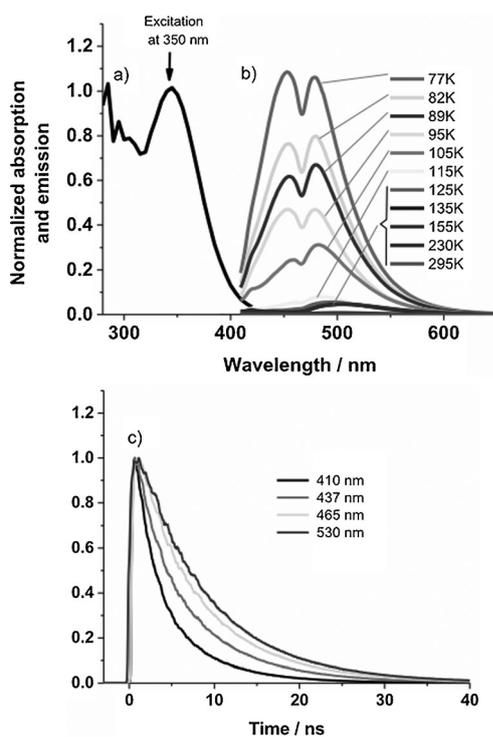

Figure 1. a) The absorption spectrum of Et-FlOH in 2-MeTHF; b) variable-temperature fluorescence spectra of Et-FlOH in 2-MeTHF; c) fluorescence decays of Et-FlOH.

The room-temperature fluorescence of Et-FlOH displays a 496 nm λ_{max} (Figure 1 b) with a Stokes shift of more than 8000 cm^{-1} and weak intensity corresponding to a quantum yield of only 3×10^{-3}.[11] The large Stokes shift and low fluorescence quantum yield are both indicative of a significant

change in geometry during the initial S_1 relaxation and following progression towards an effective radiationless decay channel. To gain a better understanding of this fast excited-state deactivation, we report a variable temperature fluorescence study of Et-FlOH. A decrease in temperature from 295 to 120 K does not affect the fluorescence intensity (Figure 1 b) consistently with an essentially barrierless S_1 nuclear motion. However, once the glass transition temperature of the solvent is reached (2-MeTHF exhibits two glass transition temperatures at 91 K and 103 K),[25] the emission intensity increases and the spectra exhibit vibronic structure with emission maxima at 437 and 465 nm. The two emission bands are assigned to the vibronic progression of the Et-FlOH excited state, as the presence of multiple conformers was ruled out based on invariant variable-temperature absorption spectra of Et-FlOH in 2-MeTHF. Furthermore, the fluorescence lifetime is increased from a 500 fs dominant component at room temperature[11] to a nanosecond biexponential decay in the glass (Figure 1 c, lifetimes are $\tau_1 = 2.8$ ns and $\tau_2 = 7.8$ ns). Such a sudden increase in the fluorescence intensity upon confinement of a chromophore in a rigid molecular cavity has also been observed in other fluorophores.[26–29] Often, this is attributed to the blocking of internal conversion mediated by a CI. However, such a CI has never been located in Et-FlOH.

A fluorescence enhancement similar to the one documented above has been observed when 4a-hydroxy flavins are protein-bound.[7,15,24,30] This suggests that confinement is also responsible for an increased S_1 lifetime in the protein cavity. However, such a mechanism would only be possible if a large change in molecular shape is required for fast internal conversion. Accordingly, we employ ab initio multiconfigurational quantum chemistry to map the S_1 relaxation path in Me-FlOH (i.e. in a slightly reduced model of Et-FlOH, see Scheme 1 a) in THF. In Figure 2 a, we present the S_0 and S_1 energy profiles along a minimum energy path (MEP) starting at the Me-FlOH Franck–Condon (FC) structure. Clearly, the MEP follows a barrierless S_1 path that eventually crosses with the S_0 state.

The analysis of the MEP shows that Me-FlOH evolves, sequentially, along two molecular modes (see also Figure S3 in the SI). First, the molecule relaxes along a bond length alternation (BLA) mode where alternating double and single bonds become elongated and shortened, respectively. This is a fast relaxation typically associated with the π,π^* excitation of π-conjugated systems.[32,33] A similar excited state relaxation was reported for lumiflavin using computations of comparable quality (i.e. with the symmetry adapted cluster-configuration interaction method).[34] After such an initial relaxation, the S_1 energy profile displays a short plateau and then continues to decrease. The MEP coordinate shows that the energy decrease is associated with an out-of-plane deformation of the pyrimidine ring with respect to the original flavin plane. Consistently, the N_1–C_{10a} bond becomes almost perpendicular to such a plane. In Figure 2 a we show that this dramatic geometrical distortion is due to the attempted isomerization about the N_{10}–C_{10a} bond that has double bond character (1.34 Å) on S_0 but becomes a single bond (1.45 Å) on S_1 after the initial BLA relaxation. Indeed,
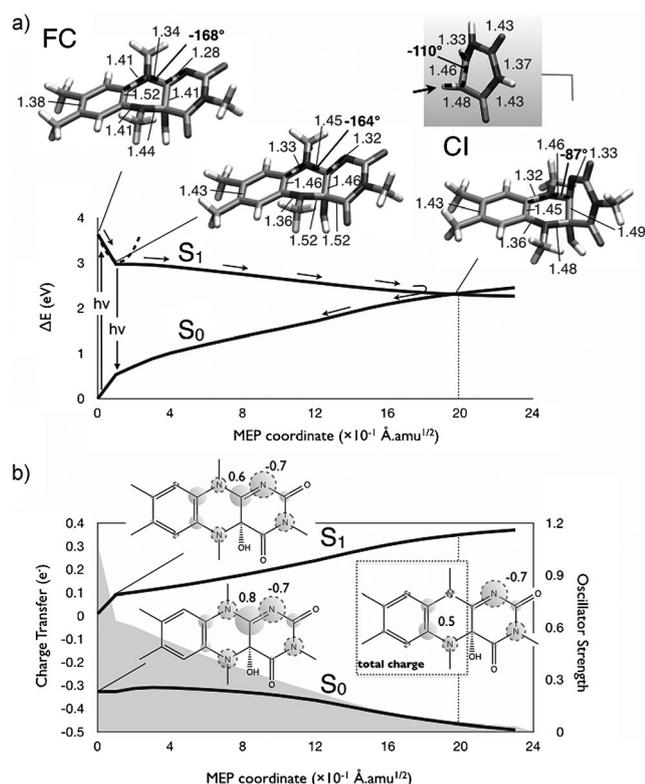
Figure 2. a) CASPT2//CASSCF S_0 and S_1 energy profiles along the MEP connecting the FC to a CI. The energy profile was computed accounting implicitly for the solvent (here we use tetrahydrofuran, THF, instead of 2-MeTHF). The bond lengths for bonds that change by more than 0.05 Å during the MEP and the dihedral angle representing the ring deformation are labeled for the FC structure, the CI, as well as for the structure reached after an initial relaxation along a stretching mode. This last structure lies on an energy plateau that may develop into a minimum on the S_1 surface (see dashed line) in the event that a barrier is introduced along the torsional deformation coordinate. The corresponding structure of the CI of uracil[31] is also shown at the top right, with the dihedral representing its torsional deformation labeled. b) Analysis of the change in S_0 and S_1 charge distributions and S_0–S_1 oscillator strength (area plot) along the MEP. The line plots represent the total charge transfer from the pyrimidine ring of Me-FlOH to the other two rings (i.e. we plot the total charge of the atoms inside the framed CI structure moiety). A more detailed charge distribution (i.e. atomistic, but with charges of substituents summed onto the backbone atoms) is shown for the S_0 state at the FC point, and for the S_1 state of the structure at the energy plateau reached by relaxation along the stretching coordinate, and for the S_1 state of the CI. Negative charges are indicated with a circle with a dashed border, while positive charges are indicated without a border. Both the S_0 and S_1 charge distributions at these geometries are shown in Figure S2 in the SI.

the C_{9a}-N_{10}-C_{10a}-N_1 dihedral angle changes from $-168°$ at the FC structure to $-87°$ at the point where the S_1 and S_0 energy profiles cross, clearly indicating a CI point. At the CI, efficient decay to S_0 takes place, eventually leading to reactant reconstitution in what may be considered an aborted N_{10}–C_{10a} isomerization.

A charge transfer process accompanies the S_1 geometrical relaxation. In fact, the Me-FlOH $S_0 \rightarrow S_1$ vertical excitation already results in the transfer of ca. $0.3\,e^-$ from the benzene and pyrazine rings to the pyrimidine ring (Figure 2b). The

charge transfer increases when the molecule relaxes along the BLA, and then continues to increase as the torsional deformation about N_{10}–C_{10a} takes place, thus placing more electron density on the pyrimidine. At the CI one reaches an overall $0.6\,e^-$ charge transfer with respect to the S_0 equilibrium structure. On the other hand, at the CI, the S_1 and S_0 electronic structures differ by a full charge transfer (i.e. changing from one state to the other would involve the translocation of $1.0\,e^-$ to the pyrimidine ring) consistently with the character of the CI's located in other biological chromophores.[35,36] The oscillator strength along the MEP also behaves as expected (orange area plot in Figure 2b). At the FC point the oscillator strength is large, but then decreases when the molecule relaxes along the BLA and reaches the energy plateau. On the plateau the oscillator strength is still large indicating possible radiative $S_1 \rightarrow S_0$ transition (i.e. fluorescence), but then it dramatically decreases along the path to the CI.

The documented Me-FlOH deactivation mechanism and CI structure may be compared with those driving the well known ultrafast internal conversion of pyrimidine nucleic acid bases (i.e. cytosine, thymine, and uracil).[31] A comparison of the CI structures of Me-FlOH and uracil[31] (see Figure 2a) shows that the reported 4a-hydroxy flavin CI represents a novel radiationless decay channel that could only exist in systems with a flavin (or lumazine) framework. In fact, the BLA pattern of the uracil CI is different (almost opposite) to that of the pyrimidine ring in the Me-FlOH CI. Furthermore, the uracil CI features a "twisted" double bond corresponding to the C_{4a}–C_{10a} bond of Me-FlOH and a highly pyramidalized (i.e. sp³ hybridized) carbon center pointing to a facile hydrogen out-of-plane twisting as indicated in Figure 2a (see the uracil structure in upper right corner. The arrow points to the displaced hydrogen). While in Me-FlOH the same bond gets partially twisted, the out-of-plane deformation is mainly due to the isomerization of the adjacent N_{10}=C_{10a} double bond as described by the C_{9a}-N_{10}-C_{10a}-N_1 dihedral in Figure 2a (see also Figure S4 in the SI for a full comparison of the geometries of the pyrimidine ring in Me-FlOH and uracil). It must be noted that the involvement of n–π* state in the deactivation, as observed for pyrimidine nucleobases,[37] is unlikely in the case of Me-FlOH. TDDFT calculations indicate that such states are too high in energy.[11]

The computations above provide a mechanism for the internal conversion of an unconfined Et-FlOH consistent with the spectroscopic features reported above. First, the observed 347 nm (3.57 eV) λ_{max} for the $S_0 \rightarrow S_1$ excitation is relatively well-reproduced by the computed 3.67 eV vertical excitation energy, and within the typical error of the employed method.[38,39] The computed deactivation path is consistent with the observed ultrafast (ca. 500 fs) S_1 lifetime in Et-FlOH,[11] and with the low (3×10^{-3}) fluorescence quantum yield, since fluorescence must compete with the internal conversion taking place at the CI.

The calculations explain the sudden increase in S_1 lifetime upon liquid to glass transition. Indeed, the MEP indicates that the S_1 deactivation in 4a-hydroxy flavins involves a large structural rearrangement from a flat to a ca. 90° bent structure. In a liquid solvent, such a distortion remains

relatively unhindered and internal conversion is allowed via the relaxation path of Figure 2 a. However, the frozen solvent would restrain the pyrimidine ring distortion. More specifically, the interaction with the solvent cavity walls would create an S_1 energy barrier immediately after the plateau seen in Figure 2 a that would then become an energy minimum (see dashed energy profile). The presence of such a barrier would then result in an increase of the S_1 lifetime and, in turn, in a higher fluorescence quantum yield. If we assume that fluorescence in the sterically constrained chromophore originates from the nearly planar system reached immediately after relaxation along the BLA mode (i.e. corresponding to the second MEP structure of Figure 2 a), then calculations predict an emission energy of 2.46 eV, which agrees with the observed fluorescence λ_{max} of 496 nm (2.50 eV) in 2-MeTHF and of 486 nm (2.55 eV) in ethanol at 77 K.[7] This also indicates that the observed 8000 cm^{-1} Stokes shift is mostly due to the relaxation of the chromophore along a BLA mode.

The same mechanism is expected to operate in luciferase. Indeed, inspection of the X-ray crystallographic data in Figure 3 reveals that the pyrimidine ring is confined in a tight
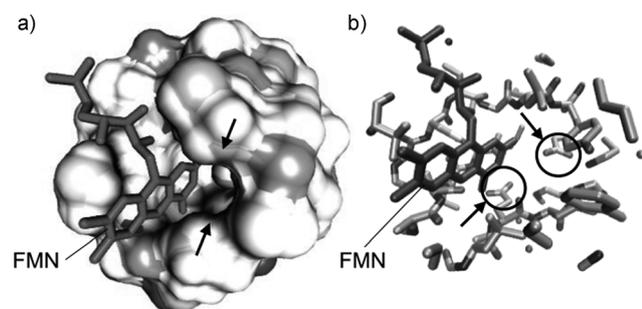
Figure 3. View of a selected portion of the 2.3 Å resolution crystal structure of the *Vibrio harveyi* luciferase:FMN complex (PDB ID: 3FGC).[40] a) The FMN structure shows that its pyrimidine ring is hosted in a tight protein cavity (see arrow). A Poisson–Boltzmann analysis,[41] based on the PROPKA (pH 7) ionization states,[42] indicates that the cavity near the pyrimidine moiety has a negative (dark gray) electrostatic potential. b) Luciferase residues surrounding the pyrimidine moiety (showing only residues within 10 Å from the C2 carbonyl carbon of the flavin moiety indicated by a red arrow) and associated with the pyrimidine cavity region. The circles point to aspartates contributing to the negative electrostatic potential.

cavity. This would restrain the ring distortion in 4a-hydroxy flavin and block the CI mediated internal conversion, thus explaining the observed high fluorescence quantum yield. Interestingly, the computed emission in THF (that is similar to the measured 2-MeTHF λ_{max}) is not far from the one observed in the luciferase of *Vibrio harveyi* (490 nm).[15,43] Our confinement hypothesis is supported by a study by Hou et al.[23] employing a TD-CAM-B3LYP based hybrid quantum mechanical/molecular mechanical model of such luciferase. It is shown that the fluorescence originates from a π,π^* 4a-hydroxy flavin with geometry and charge distribution similar to those of the second Me-FlOH structure in Figure 1 a.

In addition to steric effects, electrostatic effects may contribute to the lack of efficient internal conversion in the

protein. Indeed, the protein environment projects a negative electrostatic potential near the pyrimidine ring of the chromophore (see Figure 3 a), thus destabilizing the S_1 reaction path leading to the CI along which there is an increase in the pyrimidine negative charge (see Figure 2 b). Therefore steric and electrostatic effects together may contribute to the creation of an S_1 minimum and low tendency of the chromophore to leave such a planar fluorescent state.

Computational studies looking at the role of CIs in flavoproteins have only recently started to appear in the literature.[44] For instance, a CI mediating proton-coupled electron transfer has been proposed for blue light using flavin-adenine-dinucleotide (BLUF) domains.[44–46] Similarly, two CIs have been located in 1-deaza-FMN (1DFMN, a derivative of FMN featuring a carbon instead of a nitrogen at the N_1 position) embedded in a light oxygen voltage (LOV) domain.[47] The first CI mediates proton transfer from a thiol group to 1DFMN while the second, similar to our Me-FlOH CI but involving twisting around an adjacent bond, would provide access to a decay channel. However, the CI in Me-FlOH features an out-of-plane distortion of the entire pyrimidine ring, whereas in 1DFMN the CI has a puckering at C_1. Such a puckered CI lies ca. 1.82 eV above the FC point,[47] and it is unlikely to be relevant for the LOV domain function.

Above we have reported that the ultrafast internal conversion of S_1 4a-hydroxy flavins is controlled by accessibility to a CI lying ca. 1.30 eV below the FC point. In solution, the evolution towards the CI competes effectively with other S_1 processes such as fluorescence. However, due to the large and stiff molecular deformation required for reaching the CI, a large fluorescence enhancement is observed when 4a-hydroxy flavins are confined in a solvent glass or in the luciferase cavity. This is the first time that a CI with such a biological role has been documented for a flavin cofactor. Remarkably, this mechanism is similar to the one operating in the fluorophore of the green fluorescent protein (GFP).[48] Since GFP and luciferase appear to be chemically and biologically unrelated, one may conclude that this type of mechanism has been selected more than once during biological evolution.

The dependence of the S_1 lifetime (and therefore, fluorescence) of 4a-hydroxy flavins on their environment can make them valuable tools for probing, in real time, the changes in the flexibility or rigidity of protein active sites during processes such as catalysis, similar to studies with FMN.[2–5] Furthermore, the synthesis of novel flavin adducts coupled with mutagenesis studies may lead to novel fluorescent probes.[49] In order to drive these developments, the behavior of 4a-hydroxy flavins in solvent or protein cavities shall be further investigated/predicted using computations capable of describing the effect of the environment explicitly.

Experimental Section

Steady-State Measurements
All solvents were purchased from Sigma–Aldrich and used without further purification. The steady-state absorption spectra were recorded on a Varian Cary 50 UV/Vis spectrophotometer in a 1 cm

quartz cell. The steady-state photoluminescence spectra at room temperature and 77 K were obtained using single photon counting fluorimeter (Edinburgh Instruments FS920). The sample solutions for fluorescence measurements had absorption of 0.1–0.15 at the corresponding wavelength of excitation. Fluorescence quantum yield for Et-FlOH at room temperature was determined using argon-purged solution of $[Ru(bpy)_3](CF_3SO_3)_2$ in water as a standard ($\Phi = 0.042$).[50]

Time-resolved Photoluminescence Techniques

Low temperature fluorescence lifetimes were measured in 2-methyltetrahydrofuran using Optistat DN variable-temperature liquid nitrogen cryostat (Oxford), the gated second-harmonic (4 MHz repetition rate, 1 nJ pulse^{-1}) output of a tunable ultrafast Ti-Sapphire oscillator (Coherent, 120 fs) as an excitation source and a time-correlated single photon counting (TCSPC) detection system (Edinburgh Instruments LifeSpec II, 150 ps IRF). The excited state lifetimes were obtained from a decay fit of single wavelength emission transients using Origin 7.0 software.

Ab initio Calculations

Optimizations and MEP calculations for Me-FlOH were performed at the 2-root state-averaged CASSCF level of theory[51] with a 6-31G* basis set. The CASSCF wavefunction comprised an active space of 14 electrons in 11 orbitals (see the Supporting Information for more details on the active space). The MEP was computed with the intrinsic reaction coordinate method with a step constraint of 0.1 Bohr amu$^{-1/2}$. Single point CASPT2 calculations[52] were then performed for stationary points and for each point along the MEP path, implicitly accounting for the THF solvent using the reaction field method. The employed CASPT2//CASSCF/6-31G* protocol has been shown to be accurate for a number of organic biochromophores.[39,53,54] This protocol benefits from a cancellation of errors,[55] as discussed in the SI. The CASPT2 MEP profile of the chromophore in the gas-phase, without the effect of the solvent, is shown in Figure S6 in the SI. Mulliken charges and oscillator strengths in this work are shown for the gas-phase CASSCF level of theory. All calculations were performed with Molcas v. 7.8.[56] More details regarding the computational protocol are provided in the Supporting Information.

[1] R. Leenders, A. Van Hoek, M. Van Iersel, C. Veeger, A. J. Visser, *Eur. J. Biochem.* **1993**, *218*, 977–984.

[2] S. P. Laptenok, L. Bouzhir-Sima, J. C. Lambry, H. Myllykallio, U. Liebl, M. H. Vos, *Proc. Natl. Acad. Sci. USA* **2013**, *110*, 8924–8929.

[3] H. Yang, G. Luo, P. Karnchanaphanurach, T. M. Louie, I. Rech, S. Cova, L. Xun, X. S. Xie, *Science* **2003**, *302*, 262–266.

[4] D. Zhong, A. H. Zewail, *Proc. Natl. Acad. Sci. USA* **2001**, *98*, 11867–11872.

[5] J. Brazard, A. Usman, F. Lacombat, C. Ley, M. M. Martin, P. Plaza, L. Mony, M. Heijde, G. Zabulon, C. Bowler, *J. Am. Chem. Soc.* **2010**, *132*, 4935–4945.

[6] S. Ghisla, V. Massey, J. M. Lhoste, S. G. Mayhew, *Biochemistry* **1974**, *13*, 589–597.

[7] S. Ghisla, *Methods Enzymol.* **1980**, *66*, 360–373.

[8] C. T. Moonen, J. Vervoort, F. Mueller, *Biochemistry* **1984**, *23*, 4859–4867.

[9] C. T. Moonen, J. Vervoort, F. Müller, *Biochemistry* **1984**, *23*, 4868–4872.

[10] Y. T. Kao, C. Saxena, T. F. He, L. Guo, L. Wang, A. Sancar, D. Zhong, *J. Am. Chem. Soc.* **2008**, *130*, 13132–13139.

[11] D. Zhou, E. Mirzakulova, R. Khatmullin, I. Schapiro, M. Olivucci, K. D. Glusac, *J. Phys. Chem. B* **2011**, *115*, 7136–7143.

[12] G. Li, V. Sichula, K. D. Glusac, *J. Phys. Chem. B* **2008**, *112*, 10758–10764.

[13] J. Li, Z. Liu, C. Tan, X. Guo, L. Wang, A. Sancar, D. Zhong, *Nature* **2010**, *466*, 887–890.

[14] Y. T. Kao, C. Saxena, L. Wang, A. Sancar, D. Zhong, *Proc. Natl. Acad. Sci. USA* **2005**, *102*, 16128–16132.

[15] B. Lei, Q. Ding, S. C. Tu, *Biochemistry* **2004**, *43*, 15975–15982.

[16] S. D. Miller, S. H. Haddock, C. D. Elvidge, T. F. Lee, *Proc. Natl. Acad. Sci. USA* **2005**, *102*, 14181–14184.

[17] W. J. van Berkel, N. M. Kamerbeek, M. W. Fraaije, *J. Biotechnol.* **2006**, *124*, 670–689.

[18] J. W. Hastings, C. Balny, C. L. Peuch, P. Douzou, *Proc. Natl. Acad. Sci. USA* **1973**, *70*, 3468–3472.

[19] J. Vervoort, F. Muller, J. Lee, W. A. Van den Berg, C. T. Moonen, *Biochemistry* **1986**, *25*, 8062–8067.

[20] S. Ghisla, J. W. Hastings, V. Favaudon, J. M. Lhoste, *Proc. Natl. Acad. Sci. USA* **1978**, *75*, 5860–5863.

[21] J. W. Eckstein, K. W. Cho, P. Colepicolo, S. Ghisla, J. W. Hastings, T. Wilson, *Proc. Natl. Acad. Sci. USA* **1990**, *87*, 1466–1470.

[22] M. Kurfürst, S. Ghisla, J. W. Hastings, *Proc. Natl. Acad. Sci. USA* **1984**, *81*, 2990–2994.

[23] C. Hou, Y. J. Liu, N. Ferré, W. H. Fang, *Chem. Eur. J.* **2014**, *20*, 7979–7986.

[24] S. Ghisla, B. Entsch, V. Massey, M. Husein, *Eur. J. Biochem.* **1977**, *76*, 139–148.

[25] L. M. Wang, C. A. Angell, R. Richert, *J. Chem. Phys.* **2006**, *125*, 074505.

[26] J. Grilj, E. N. Laricheva, M. Olivucci, E. Vauthey, *Angew. Chem.* **2011**, *123*, 4589–4591; *Angew. Chem. Int. Ed.* **2011**, *50*, 4496–4498.

[27] D. F. Duxbury, *Chem. Rev.* **1993**, *93*, 381–433.

[28] A. Nakayama, T. Taketsugu, *J. Phys. Chem. A* **2011**, *115*, 8808–8815.

[29] K. L. Litvinenko, N. M. Webber, S. R. Meech, *J. Phys. Chem. A* **2003**, *107*, 2616–2623.

[30] K. Detmer, V. Massey, *J. Biol. Chem.* **1984**, *259*, 11265–11272.

[31] M. Merchán, R. González-Luque, T. Climent, L. Serrano-Andrés, E. Rodríguez, M. Reguero, D. Peláez, *J. Phys. Chem. B* **2006**, *110*, 26471–26476.

[32] R. González-Luque, M. Garavelli, F. Bernardi, M. Merchán, M. A. Robb, M. Olivucci, *Proc. Natl. Acad. Sci. USA* **2000**, *97*, 9379–9384.

[33] M. Drobizhev, T. E. Hughes, Y. Stepanenko, P. Wnuk, K. O'Donnell, J. N. Scott, P. R. Callis, A. Mikhaylov, L. Dokken, A. Rebane, *Sci. Rep.* **2012**, *2*, 688.

[34] J. Y. Hasegawa, S. Bureekaew, H. Nakatsuji, *J. Photochem. Photobiol. A* **2007**, *189*, 205–210.

[35] L. Salem, *Acc. Chem. Res.* **1979**, *12*, 87–92.

[36] P. B. Coto, A. Sinicropi, L. De Vico, N. Ferre, M. Olivucci, *Mol. Phys.* **2006**, *104*, 983–991.

[37] M. Barbatti, A. J. Aquino, J. J. Szymczak, D. Nachtigallová, P. Hobza, H. Lischka, *Proc. Natl. Acad. Sci. USA* **2010**, *107*, 21453–21458.

[38] D. Roca-Sanjuán, F. Aquilante, R. Lindh, *WIREs Comput. Mol. Sci.* **2012**, *2*, 585–603.

[39] I. Schapiro, M. N. Ryazantsev, W. J. Ding, M. M. Huntress, F. Melaccio, T. Andruniow, M. Olivucci, *Aust. J. Chem.* **2010**, *63*, 413–429.

[40] Z. T. Campbell, A. Weichsel, W. R. Montfort, T. O. Baldwin, *Biochemistry* **2009**, *48*, 6085–6094.

[41] N. A. Baker, D. Sept, S. Joseph, M. J. Holst, J. A. McCammon, *Proc. Natl. Acad. Sci. USA* **2001**, *98*, 10037–10041.

[42] M. H. M. Olsson, C. R. Søndergaard, M. Rostkowski, J. H. Jensen, *J. Chem. Theory Comput.* **2011**, *7*, 525–537.

[43] T. W. Cline, J. W. Hastings, *J. Biol. Chem.* **1974**, *249*, 4668–4669.

[44] T. Domratcheva, A. Udvarhelyi, A. R. Shahi, *Methods Mol Biol* (Ed.: J. M. Walker), Springer, New York, **2014**, pp. 191–228.

[45] A. Udvarhelyi, T. Domratcheva, *Photochem. Photobiol.* **2011**, *87*, 554–563.

[46] K. Sadeghian, M. Bocola, M. Schütz, *Phys. Chem. Chem. Phys.* **2010**, *12*, 8840–8846.

[47] M. R. Silva-Junior, M. Mansurova, W. Gärtner, W. Thiel, *ChemBioChem* **2013**, *14*, 1648–1661.

[48] M. E. Martin, F. Negri, M. Olivucci, *J. Am. Chem. Soc.* **2004**, *126*, 5452–5464.

[49] A. Mukherjee, K. B. Weyant, J. Walker, C. M. Schroeder, *J. Biol. Eng.* **2012**, *6*, 20.

[50] A. Juris, V. Balzani, F. Barigelletti, S. Campagna, P. L. Belser, A. Von Zelewsky, *Coord. Chem. Rev.* **1988**, *84*, 85–277.

[51] B. O. Roos in *Advances in Chemical Physics*: *Ab Initio Methods in Quantum Chemistry Part 2*, *Vol. 69* (Ed.: K. P. Lawley), Wiley, **1987**, pp. 399–445.

[52] K. Andersson, P. A. Malmqvist, B. O. Roos, A. J. Sadlej, K. Wolinski, *J. Phys. Chem.* **1990**, *94*, 5483–5488.

[53] P. Z. El-Khoury, I. Schapiro, M. Huntress, F. Melaccio, S. Gozem, L. M. Frutos, M. Olivucci in *CRC Handbook of Organic Photochemistry and Photobiology* (Eds.: A. Griesbeck, M. Oelgemoller, F. Ghetti), CRC, Taylor & Francis, Boca Raton, **2012**, pp. 1029–1056.

[54] S. Gozem, F. Melaccio, H. L. Luk, S. Rinaldi, M. Olivucci, *Chem. Soc. Rev.* **2014**, *43*, 4019–4036.

[55] S. Gozem, M. Huntress, I. Schapiro, R. Lindh, A. A. Granovsky, C. Angeli, M. Olivucci, *J. Chem. Theory Comput.* **2012**, *8*, 4069–4080.

[56] F. Aquilante, L. De Vico, N. Ferré, G. Ghigo, P. A. Malmqvist, P. Neogrády, T. B. Pedersen, M. Pitonák, M. Reiher, B. O. Roos, L. Serrano-Andrés, M. Urban, V. Veryazov, R. Lindh, *J. Comput. Chem.* **2010**, *31*, 224–247.